Lipid perturbation by membrane proteins and the lipophobic effect

James N. Sturgis, Jean-Pierre Duneau, Jonathan Khao

Lipid perturbation by membrane proteins and the lipophobic effect

Jean-Pierre Duneau[a,*], Jonathan Khao[a,1], James N. Sturgis[a]

[a]*Laboratoire d'Ingénierie des Systèmes Macromoléculaires, UMR 7255, CNRS and Aix-Marseille Univ, Marseille, 13402 cedex 20, France*

Abstract

Understanding how membrane proteins interact with their environment is fundamental to the understanding of their structure, function and interactions. We have performed coarse grain molecular dynamics simulations on a series of membrane proteins in a membrane environment to examine the perturbations of the lipids by the presence of protein. We analyze these perturbations in terms of elastic membrane deformations and local lipid protein interactions. However these two factors are insufficient to describe the variety of effects that we observe and the changes caused by membranes proteins to the structure and dynamics of their lipid environment. Other factors that change the conformation available to lipid molecules are evident and are able to modify lipid structure far from the protein surface, and thus mediate long-range interactions between membrane proteins. We suggest that these multiple modifications to lipid behavior are responsible, at the molecular level, for the lipophobic effect we have proposed to account for our observations of membrane protein organization.

Keywords: molecular dynamics simulation; lipid structure; biological membranes; protein-lipid interactions

Introduction

Biological membranes are complex structures that form the barrier between the living cell and its environment. The protein and lipid components of the membrane organize themselves to form a dynamic 2D fluid, the structure and function of which is vital for life. Within this membrane, lipids, through their influence on the proteins, are important in membrane protein insertion [1–4], folding [4, 5], assembly into larger complexes [6, 7] and activity [8–10]. It is thus important to understand the complexity of lipid-protein interactions to decipher the interplay between protein sequences in one hand and the lipid composition on the other hand.

Current understanding of interactions between membrane proteins and their lipid environment comes from two different schools. First a mechanical elastic vision pioneered by Helfrich [11] considers the lipid membrane as an elastic sheet that is more or less deformed by curvature. This planar two dimensional vision was extended by the membrane mattress model [12] where the sheet was given thickness and embedded proteins. In this field view, the membrane perturbations are described in terms of hydrophobic mismatch [12–16] or curvature mismatch [17–22]. In both cases these are envisioned as a mismatch between the local lipid properties and those of the embedded proteins.

A second view relies on a chemical and molecular description where interactions and perturbations are seen as the affinity or binding of specific lipids or lipid classes to the membrane protein surface [23–25], and additionally the existence of annular lipids [26–28] with modified structure and dynamics. In this descriptions protein–protein interactions are influenced by modifications to both lipid packing and the annular lipid preferences [29]. This situation is similar to the solvation water found around soluble proteins which has modified structure and dynamics. The differences between the water and water far from solutes are responsible for the hydrophobic effect. Some of these changes in molecular properties of the solvent can be observed by experimental measures, such as the measurement of the nmr order parameter S_{CD}[30].

These two visions can both accommodate the possibility that the membrane contains regions with different chemical composition and mechanical properties, notably the existence of more or less stable domains or phase separated regions [20].

Despite its success in describing forces that arise from perturbation of the pure lipid membrane properties, the elastic description concerns a very abstract protein described essentially as a hydrophobic conical segment that gives little place to local interactions. In particular it can not represent the effect of the topography of protein surfaces.

The molecular view is increasingly extended, especially by integrating aspects that initially came from elastic models. However the description of the molecular perturbations at the origin of long range interactions is complex. An important question not currently be treated is how the modulation of membrane protein properties could influence long range interaction for example for the control of

*Corresponding author

[1]Current address: Digizyme, 154 Chemin de Sormiou, 13009 Marseille, France.

supra-molecular assembly [31].

Among the tools that have recently advanced our understanding of membrane protein assembly are molecular dynamics simulations. Such simulations have been able: to successfully reproduce specific lipid binding sites seen in electron diffraction experiments [32, 33]; and to describe, at atomic resolution, some of the perturbation associated to the lipid annulus [34], including the reproduction of NMR order parameters. This coming of age of chemical simulation is the result of the attractive molecular vision that can be provided, the maturity of the force fields that have been developed, and a wider appreciation of their power and limitations [35–41].

Despite these advances, classical chemical simulations are hard to use on the time-scale (10 to 100 μs) frequently required for the description of complex biomolecular system. Fortunately, coarse grain (CG) molecular dynamics simulations have demonstrated their ability to reproduce many such phenomena. CG simulations of lipids have been used to: study phase transitions [42, 43]; lipid (de)mixing [44, 45]; or vesicles dynamics [46, 47]. Many aspects of lipid–protein interactions have also been reproduced in CG simulaions despite the reduction of resolution and the simplification of the energy potential [48–52]. Such simulations have also been used to successfully study membrane protein interactions [52–56].

In this article we describe coarse grained (CG) molecular dynamics simulations of eleven different membrane proteins in a phospholipid bilayer and analyze them in order to describe how membrane proteins perturb their environments. Our objective has been to understand how membrane proteins interact with their lipid environment, the nature of the perturbations and the relative importance of the different parameters that have been proposed. Recently we proposed a lipophobic effect [31], in part as an extension and generalization of hydrophobic and curvature mismatch, to explain our observations of membrane protein organization [57]. This term has also been recently used to describe various related aspects of protein-lipid interactions [29, 58]. Much as the understanding of soluble protein folding depends on our understanding of the physical-chemical basis of interactions with their solvent particularly water through the hydrophobic effect [59] we believe that understanding of membrane proteins will depend on our understanding of their interactions with a more complex solvent and this lipophobic effect.

Methods

System setup

The biological units of the various proteins were selected from our non-redundant database of membrane proteins (NORM) [60]. The proteins selected (table 1) corresponds to proteins of various sizes originating in different organisms and hence chemically diverse membranes. However, 8 of the 11 proteins come from the inner membrane of Gram negative bacteria. Based on this we decided to model the different membrane proteins in a membrane composed of 80% palmitoyl-oleyl-phosphatidyl-ethanolamine (POPE) and 20% palmitoyl-oleyl-phosphatidyl-glycerol (POPG). This mixture, much simpler in lipid composition than a natural membrane, is expected to produce a membrane of approximately the correct thickness and with an appropriate balance of anionic and zwitterionic head groups [44, 61, 62].

The membrane was constructed from a preformed 128 lipid POPE bilayer (wcm.ucalgary.ca/tieleman/) as follows. We used the "martinize" script, available from the Martini web site [63] (www.cgmartini.nl) to convert the resulting all atom structure into its coarse grain counterpart. Then randomly selected lipids were converted from POPE to POPG by deleting the single coarse grain particle that differentiates the two lipid types. The resulting structures for simulation were energy minimized (using 5000 steps of the steepest descent algorithm), thermalized at 326K to ensure bilayer fluidity in Martini throughout equilibration, and equilibrated over 4 μs using Gromacs [64]. The resulting membrane thickness, calculated between the N beads of the POPE in each leaflet, is on average 4.45 nm. This is exactly the same as the distance computed from a published all atom simulation [62] and at the upper range of another series of simulation [44].

Then, the protein and the equilibrated CG membrane were fused using the g_membed tools [65] available with Gromacs 4.6. In all simulations, the dynamics of the proteins subunits were corrected using the ElneDyn elastic network [66].

Simulations

Standard parameters for Martini simulation were used, including a 20 fs time step, the temperature was controlled at 300K using the Berendsen algorithm [67] with a time constant of 0.5 ps. The pressure was maintained at 1 bar in semi-isotropic condition with the Berendsen algorithm [67] and a time constant of 1.2 ps. Van der Waals and electrostatic interaction are calculated using a shift function from 0.9 to 1.2 nm and 0.0 to 1.2 nm respectively. The same parameters were used for all simulated systems. The various systems listed in table 1 were simulated over 10 μs at the CINES facility.

Analyses

For the calculation of the occupancy, the frames of the trajectory are fitted to the first frame of the simulation based on the protein position. In this initial frame the membrane normal was aligned along the z axis, and the center of mass of the protein located at the origin. With this fitting, structural properties of the membrane can be located in a semi-polar coordinate system expressed relative to the center of mass of the membrane protein and the membrane normal. We termed polar averages the quantities that were averaged in this coordinate system. The

average occupancy are calculated in 3D at each node of a 0.2 nm spaced grid using the volmap tool available in VMD [68]. The particle occupancies are averaged over 5000 frames spanning the full 10 μs simulation time. The volmap tool was used to produce density profiles for each type of lipid particle at various distance from the protein surface. The projection of these profile onto the z axis gives the transbilayer density profiles. These profiles were used to calculate the membrane thickness, defined as the distance between density maxima for the glycerol beads in each of the leaflets, and the membrane midplane position, using the center of the last acyl chain bead distribution. The lipid positions in the membrane plane, were analyzed by projecting the phosphorus positions onto the plane of the corresponding monolayer.

Results

We constructed coarse grained models of a series of α-helical membrane proteins (see table 1) embedded in a lipid bilayer, and performed molecular dynamics simulations over 10 μsec. Examination of these trajectories allows us to study how lipid structure and dynamics are modulated by the presence of the membrane proteins, while the simulation of multiple different proteins allows us to investigate the effects of various protein parameters. The proteins we simulated were extracted from a database of non-redundant membrane protein structures [60]. Our selection was made to balance structural diversity, on the one hand, with the inclusion of several examples of structurally similar proteins, on the other hand. Thus in our selection there are 3 members of the aquaporin family: Aquaporin M; the glycerol facilitator GlpP; and the spinach aquaporin SoPiP2.

These simulations were designed to allow us to investigate the response of a phospholipid bilayer of constant composition to a series of proteins with different shapes and surfaces.

The molecular view

In common with previous investigations using all atom representations of lipids [82], we observe multiple lipid residence sites on the surface of all the proteins investigated. In figure 1A we show regions with excess lipid density observed on the surface of the potassium transporter KcsA. As can be clearly seen the various sites do not show the binding of entire lipid molecules but of different parts of the lipid acyl-chains, leaving the rest of the molecule flexible. While in some cases, notably aquaporins, long high density regions representing the major part of acyl chains are observed, as previously reported [82], more usually a patchy and discontinuous series of densities, as shown here, was observed. This appears to indicate that parts of the lipid molecule are relatively well bound to the protein surface while other portions remain flexible. The lipid binding regions detected share the symmetry of the proteins, as shown in supplementary figure S1, this is a good indication that the simulations have converged.

Illustrated in figure 1B are a selection of conformations of single lipid molecules occupying one of these sites. These images show that while lipids are preferentially found at this position on the protein surface it does not really represent part of a specific binding site, but rather something much less fixed. Each location associating with sequentially with different chemical groups of the phospholipid and with the lipid molecule in very different conformations. For example, in the second frame the palmitoyl SN1 chain of the lipid is bound to the protein while in the others the oleyl (SN2) chain is associating with the protein. Furthermore, the depth of the double bond (pink bead) in the membrane is variable being much closer to the membrane surface in the fourth image than the third. As a final example of the variability of lipid conformations we can point out the positioning of the non-bound acyl-chain. It is in an almost parallel conformation in the second image, and a very spread conformation in the fourth panel. It is interesting to note that the the instantaneous conformations shown each represents a different lipid molecule, ie after exchange with the rest of the lipids. The trajectories of several of these lipid molecules are shown in the supplementary figure S2, to illustrate how over the course of the simulation the lipids can exchange and diffuse long distances visiting multiple different sites on the protein. Thus, while the site shown is preferentially occupied by lipids, with an acyl-chain running down the surface of the protein, the bound lipid remains very flexible in the site, changing conformation rapidly, and exchanging with other lipids. The average residence time for a lipid is only about 150 ns in the site shown, reinforcing the idea that lipids are not immobilized on the surface in specific binding sites.

Drawing on this analysis, and profiting from the longer integration times possible in coarse-grained simulations, we have extended this analysis to study more subtle density fluctuations around the different proteins. In figure 2 we show on the left (panels A to I) these particle density fluctuations as a function of depth and position in the membrane around the spinach aquaporin SoPIP2. In this illustration surface binding sites or preferential localization sites are again clearly visible, as greenish spots near the protein-lipid interface (see for example black arrow in panel F). It is apparent in this view that these sites do not necessarily correspond to depressions on the surface, indeed some of them appear to be associated with ridges (black arrow), while others (as in figure 1) are more understandably associated with surface depressions (white arrow in panel G). Also visible in this figure is the distance that the ordering of lipid molecules extends around the protein. This is apparent as colored density ripples in the membrane. These ripples represent successive solvation shells, and often suggest 4 to 5 solvation shells around the protein at certain depths, extending out to about 1.5 nm from the protein surface. A further point in this part of the figure that merits comment is the heterogeneity of

Protein Name	PDB code	Gyration Radius of oligomer (nm)	Hydrophobic thickness (nm)	Reference
CIC Chloride Channel	(PDB ID:1OTS)	1.71	2.97	[69]
Aquaporin M	(PDB ID: 2F2B)	1.55	2.90	[70]
Sodium/Proton Antiporter	(PDB ID: 1ZCD)	1.17	2.84	[71]
Glycerol facilitator	(PDB ID: 1FX8)	1.78	3.01	[72]
Spinach Aquaporin	(PDB ID: 1Z98)	1.66	2.81	[73]
Lactose permease	(PDB ID: 1PV6)	1.1	3.19	[74]
Glycerol-3-Phosphate Transporter	(PDB ID: 1PW4)	1.13	3.12	[75]
Vitamin B_{12} ABC Transporter	(PDB ID: 1L7V)	1.52	3.07	[76]
Mitochondrial ATP/ADP carrier	(PDB ID: 1OKC)	1.1	2.95	[77]
Potassium channel KcsA	(PDB ID: 1R3J)	1.06	3.48	[78]
Neurotransmitter transporter	(PDB ID: 2A65)	1.22	2.98	[79]

Table 1: The proteins that have been studied in this article. For each of the proteins examined we show, the structure taken from the PDB along with the associated reference, and the size which was determined using the g_gyrate module from the Gromacs program suites[64] and hydrophobic thickness obtained from PDBTM/TMDET [80, 81].

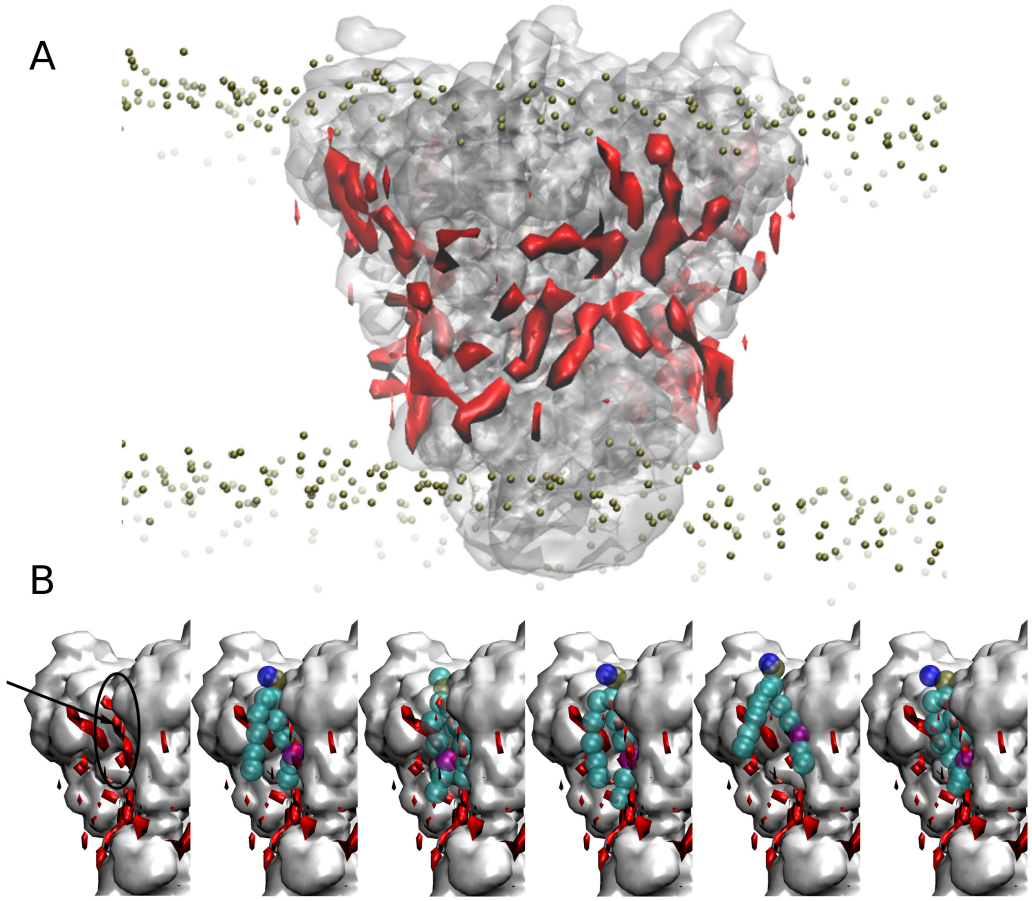

Figure 1: Lipids on the surface of the Potassium channel KcsA. A. Lipid locations on the surface of the protein. Particle densities were averaged from 2500 frames sampled from the 10 μs of simulation. The red surfaces show zones of density greater than 1.36 times the average lipid particle density in the membrane. To highlight the boundaries of the lipid bilayer, the phosphate particles of all the lipids in one frame are shown as a greenish spheres. B. Gallery of five instantaneous lipid conformation showing lipids occupying the site indicated in the left-hand panel. In these images CG beads are colored according to their chemical type as follows: head-group, blue; glycerol, green; saturated acyl-chain, turquoise; unsaturated section, pink.

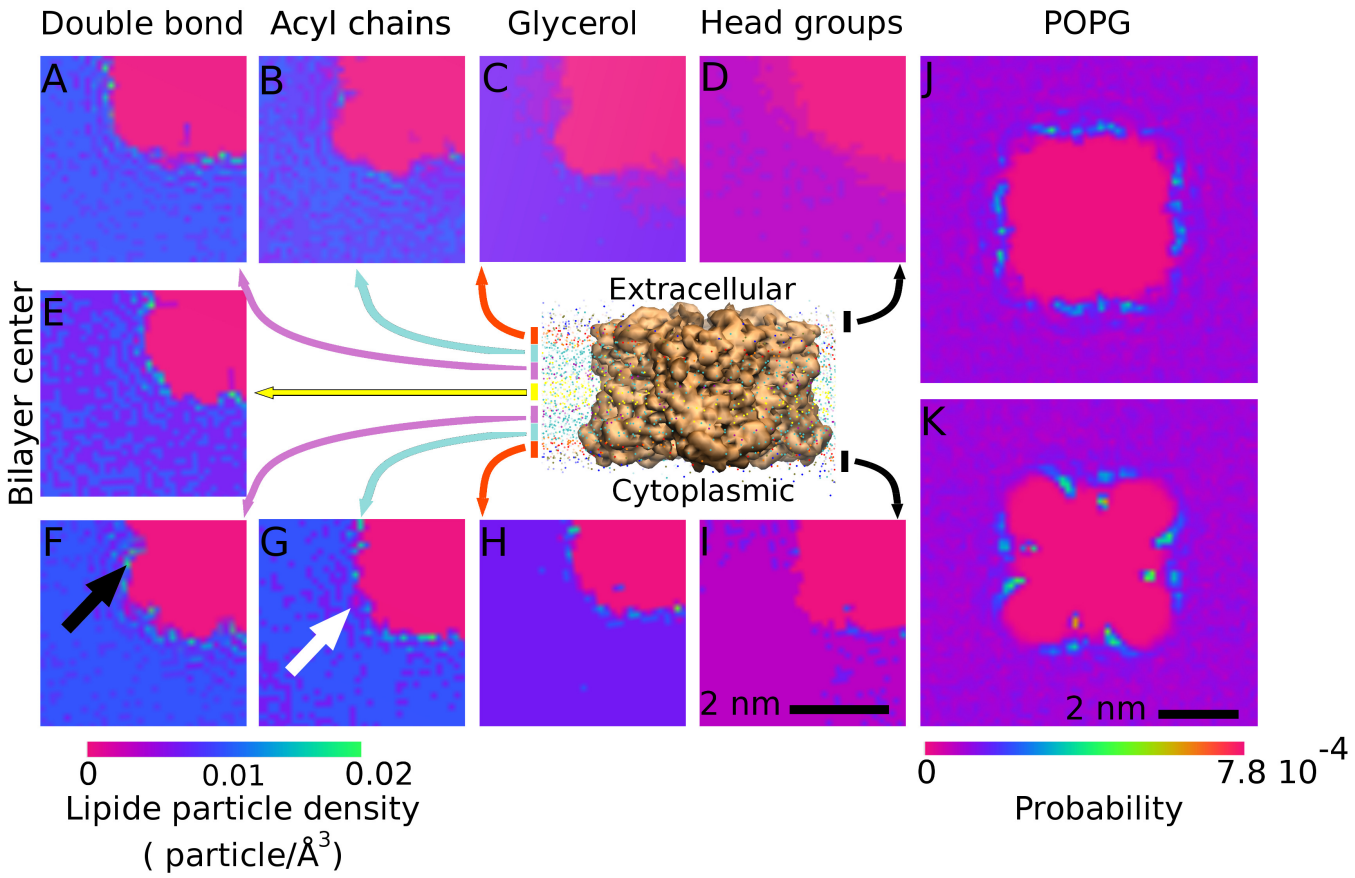

Figure 2: Left hand panels (A to I) and diagram, lipid particle densities at various depths in the membrane around the spinach aquaporin. Each map is colored to show the particle density from green high density through blue to red low density. Particles densities were calculated using 5000 frames from a 10 μs simulation. Each particle in every frame was binned using the volmap tool of vmd at 2Å resolution in a 3D matrix. Each map corresponds to distinct volume slices (2Å thick) at different depths in the membrane. Right hand panels (J and K), preferential selection of POPG close to the spinach aquaporin protein surface. The top (J) and bottom (K) panels show the probability of finding POPG in the extracellular (trans) and intracellular (cis) leaflet respectively at the given location. The position of the phosphate group were extracted from 10000 frames in the 10 μs simulation and binned in a 150 x 150 matrix that samples the 30 x 30 nm membrane plane. The integral over the bins were normalized to 1 to give a probability density function.

the slices, the slices at all depths do not appear the same, even slices at the same depth in different leaflets are different. It is important to insist also that these positional perturbations are associated with the structure of the protein. Smooth solvation shells are not observed but rather a speckled appearance with preferred positions reminiscent of an interference pattern of waves reflected from a surface that varies with depth.

The maps on the right hand side in figure 4 (panel J and K) show lipid head-group sorting due to the presence of the protein; top (J panel) and bottom (K panel) correspond to the outer (trans) and inner (cis) leaflet respectively. Illustrated is the probability of finding a POPG molecule, which is the less common lipid in our modeled membrane. It is also apparent from this figure that the observed fluctuations have converged as the maps are very similar on the different surfaces of the symmetric protein thus preserving the symmetry. Here we see a strong preference for the anionic lipid POPG at certain positions round the protein, presumably resulting largely from the electrostatics of the protein surface. Interestingly we can observe, particularly in the upper panel, that this preference extends beyond the first solvation shell.

This molecular view thus illustrates the presence of sites on the protein surface capable of binding selected lipids. Theses include those leading to weak diffuse binding of acyl-chains, or parts of acyl-chains, and those preferentially binding certain head-groups. Beyond these specific sites in the first solvation layer we observe multiple solvation layers around the protein forming a complex structure in a three dimensional pattern. Bound lipids or preferred lipid locations and solvation shells both represent restrictions in the positional freedom of the lipids. These are aspects of solvent ordering typical of a molecular view, and are excluded from the elastic vision of a membrane.

The elastic view

The simulations also allow us to evaluate the elastic deformations of the membrane. To estimate the hydrophobic mismatch of the various proteins, and their influence on membrane curvature. This information is included in figure 3, table 2 and supplementary figures S3 and S4. The panels A and B, of figure 3, show how the thickness of the membrane, which is thinned next to the protein due to hydrophobic mismatch, relaxes with distance from the protein. The points show the calculated average thickness at different distanced from the proteins, while the curve shows a exponential fit to the data. As can be readily seen, and is expected, at large distances the thickness relaxes in an approximately exponential manner with a characteristic length scale of 0.50 nm. All the different proteins give a similar length scale for this thickness relaxation ($0.49 \pm 0.10nm$), when this parameter was adjusted independently for the different proteins. Similarly the membrane thickness at long distances always relaxes to the same value ($3.57 \pm 0.09nm$). This is expected as all the different proteins are embedded in a membrane with the same composition, and thus with the same elastic properties and intrinsic thickness. However, close to the protein the relaxation is more complex (panel B). Indeed, extrapolation of the long range exponential decay to the protein surface gives a very thin and unrealistic limit of 0.64 to 2.04 nm (table 2 column 2), depending on the protein considered, all the hydrophobic mismatches are negative in our study. Examination of the fits close to the protein surface (below about 0.75nm), figure 3B, and supplementary figure S3B and D, show that there are considerable local deviations which depends on the protein. This illustrates that in this region, close to the protein, the membrane can not be reasonably modeled as a simple centro-symmetric elastic medium deformed by the protein.

To better understand these deviations we considered the predicted thickness of the first shell of lipids, which is typically at a distance of 0.5 nm (table 2 column 3), and compare it to the thickness calculated in the simulation (column 4). It is readily apparent that there is little correlation between these 2 columns, indeed they appear anti-correlated (Spearman rank correlation -0.81). This suggests the elastic (exponential) extrapolation to short distances exaggerates the hydrophobic mismatch. As a result, at short distances, the thickness extrapolated from the elastic relaxation does not match that found in our CG calculation.

The comparison of the values seen in our CG simulations, $CG_{0.5}$, with those given by PDBTM and OPM as the hydrophobic thickness shows a very close agreement, especially between estimates by the PPN algorithm in the OPM database and our calculation. For example the average thickness values are almost identical, 3.04 ± 0.13 and 3.03 ± 0.19 nm respectively, and the root mean square difference is only 0.04 nm. This correspondence is also supported by good correlation between the series (Spearman correlation coefficient 0.78). The agreement with PDBTM is slightly less good, though still reasonable. It is noteworthy that the PNM algorithm does not a attempt to calculate the hydrophobic thickness of membrane proteins. Instead it consider the partitioning of surface residues and a continuum model of membrane to calculate a position equilibrium for the first lipid shell. So it is reassuring that CG models give very similar results.

This analysis shows that the simulations reveal an important hydrophobic mismatch with adjustment of membrane thickness round the protein. This hydrophobic mismatch is typically envisioned as an elastic deformation projected from the protein surface, however our observations would tend to suggest the projected relaxation is perhaps best viewed as coming from the first solvation layer where specific interaction between lipids and the protein surface strongly influence lipid positioning and hide the simplistic hydrophobic thickness.

To further describe the physical adaptation of the membrane to the protein surfaces we calculated the position of the membrane "mid-plane" using the density of the lipid tips (see methods). It was not possible to define the curva-

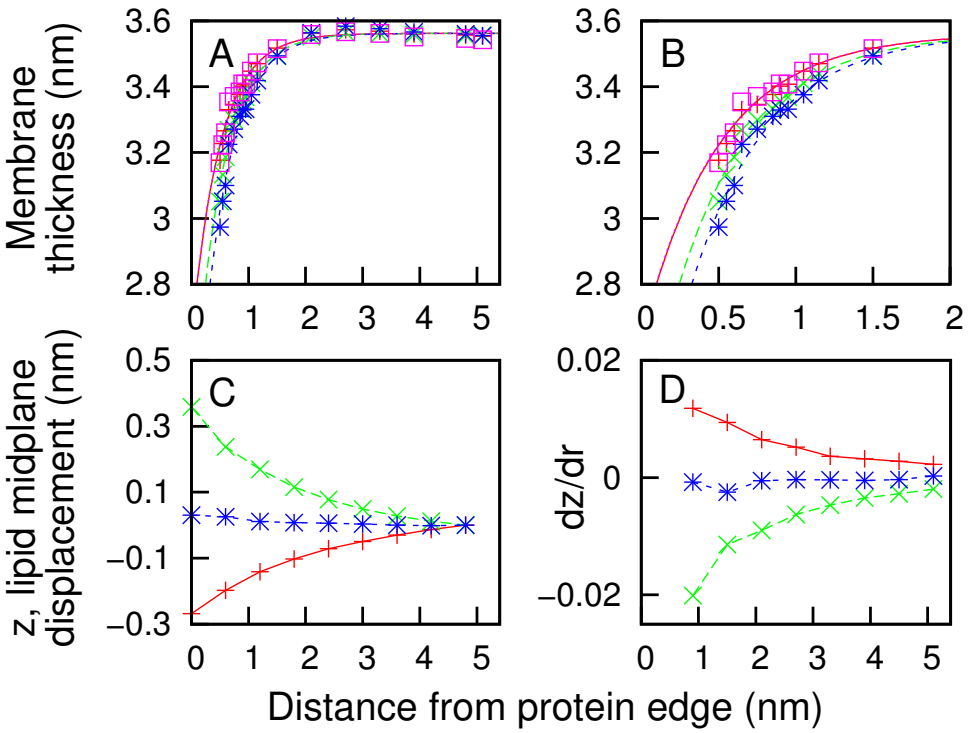

Figure 3: Relaxation of membrane thickness and position of the mid-plane as distance from the protein surface increases. Membrane thickness, panels A and B, was calculated as the distance between the glycerol moieties of the phospholipids and is show as a function of the distance from the protein surface. The lines show exponential fits to the data with the parameters shown in table 2. For clarity the figure here shows data for 4 proteins: vitamin B_{12} ABC transporter (PDB ID: 1L7V, red), Mitochondrial ATP/ADP carrier (PDB ID: 1OKC, green), CIC Chloride channel (1OTS, blue) and Lactose permease (PDB ID: 1PV6, magenta). The supplementary figure S3 shows equivalent data for the other proteins studied. Panel A shows data going out to long distances while panel B concentrates on the distortions close to the protein. Membrane curvature, panels C and D. Displacement of the membrane mid-plane (panel C) was calculated assuming a centro-symmetric model as a function of distance from the protein center, and the derivative of this with distance (panel D). For clarity the figure here shows data for 3 proteins: Lactose permease (PDB ID: 1PV6, red), Potassium channel KcsA (PDB ID: 1R3J green), and Glycerol falicitator (PDB ID: 1Z98, blue). See the supplementary figure S4 for an equivalent figure with data for the other proteins studied.

Protein Name	Hydrophobic thickness (nm)				
	$E_{0.0}$	$E_{0.5}$	$CG_{0.5}$	PDBTM	OPM
CIC Chloride Channel (PDB ID: 1OTS)	1.47	2.23	2.97	2.10	2.97
Aquaporin M (PDB ID: 2F2B)	2.00	2.54	2.85	2.55	2.90
Sodium/Proton Antiporter (PDB ID: 1ZCD)	1.92	2.53	2.84	2.60	2.84
Glycereol facilitator (PDB ID: 1FX8)	1.17	2.05	3.11	2.60	3.01
Spinach Aquaporin (PDB ID: 1Z98)	1.14	2.03	3.00	2.65	2.81
Lactose permease (PDB ID: 1PV6)	0.92	1.89	3.17	3.05	3.18
Glycerol-3-Phosphate Transporter (PDB ID: 1PW4)	0.64	1.71	3.21	3.20	3.12
Vitamin B_{12} ABC Transporter (PDB ID: 1L7V)	0.92	1.89	3.18	3.25	3.07
Mitochondrial ATP/ADP carrier (PDB ID: 1OKC)	1.25	2.10	3.05	3.30	2.95
Potassium channel KcsA (PDB ID: 1R3J)	1.85	2.48	3.12	3.45	3.48
Neurotransmitter transporter (PDB ID: 2A65)	2.04	2.60	2.98	2.95	2.98
Average	1.39	2.19	3.04	2.88	3.03
Standard deviation	0.49	0.31	0.13	0.41	0.19

Table 2: Fitted of elastic membrane parameters for the different proteins. The calculated membrane thickness at different distances from the protein surface was fit to a single exponential function. The value for $Thickness_{\infty}$ and characteristic relaxation length were fitted globally, the same for all proteins, to 3.56 nm and 0.50 nm respectively. Values for the extrapolated hydrophobic thickness at the protein surface $E_{0.0}$ and at 0.5 nm, the first solvation layer, $E_{0.5}$ are tabulated, followed by the thickness calculated for this first lipid shell $CG_{0.5}$. Finally hydrophobic thickness determined by PDBTM [81] and OPM [83] are also tabulated.

ture of those plane because it is locally very close to zero. However we could calculate a variation of the tip position as a function of distance from the protein 3C.

The three proteins illustrated caused membrane adaptation of various degrees. Curves for the remaining proteins are shown in supplementary figure S4. For example KcsA (PDB ID: 1R3J) and lactose permease (PDB ID: 1PV6) induce a large displacement in the position of the midplane while for the spinach aquaporin (PDB ID: 1Z98) almost no perturbation is observed. These curvatures are fully in line with the form of the proteins, i.e. an enlarged membrane spanning domain on the periplasmic side for KcsA, the cytoplasmic size for the lactose permease structure and a very symmetric structure for the aquaporin. For all the proteins that induced membrane curvature, at long distances, greater than about 2.5 nm this relaxes more or less exponentially. This relaxation results from the interplay of bending rigidity and membrane tension.

As for the membrane thickness, at shorter distances behavior is much more varied, showing peaks or troughs and sudden departures from the expected elastic relaxation. This is particularly visible in the slope of the change of the membrane midplane position (Fig 3D). For example in the case of the aquaporin with an apparent stepwise shift in the midplane position at 1.2 nm form the protein surface. This would seem to indicate that membrane curvature close (<2.5 nm) to the protein is modulated by effects other than a simple relaxation induced by the mismatch between the protein hydrophobic surface and the membrane normal. However we were unable, as in the case of the membrane thickness to find a simple explanation for the varied behavior we observed.

This elastic analysis reveals that while at long distances from the protein the membrane thickness and curvature behave as predicted by a simple elastic model closer to the protein more specific effects are at play with the proteins significantly modifying the elastic properties of the membrane in their vicinity. As predicted by elastic models and observed, the perturbations caused to membrane thickness and curvature return to their intrinsic values over the first few nm.

Other long range effects

To further characterize the structural modifications of the lipids around the various membrane proteins, we analyzed the depth in the membrane of each of these beads (Heads, Glycerol and Unsaturation groups) this for each of the two membrane leaflets (figure 4). The three proteins illustrated show rather different behaviors. In the case of the glycerol facilitator GlpF, panel 4A and 4B the three beads behave in essentially the same manner. The positions can be seen to relax more or less homogeneously with characteristic distances of several nm, here, though there is a small deviation for the unsaturation close to the protein surface. In the case of the neurotransmiter transporter, panels 4C and 4D while the glycerol and head group relax together the length scales are rather different on the two leaflets, and the relaxation of the double bond position is complex (not a simple exponential) and has a very long characteristic distance more than 3 nm in the outer leaflet. Finally for the lactose permease shown in panels 4E and 4F we again see complex effects, in particular for the position of the double bond.

The relaxation in the positions of the glycerol and phosphate positions largely reflects the relaxation of membrane thickness and curvature around the protein. It is hard to understand, at the molecular level, why the perturbations affecting the position of the unsaturated bond relax in such an unexpected manner, and persist to such large distances from the protein. We were unable to identify particular structural metrics that were perturbed, for example the order parameter if the oleyl chains are not markedly modified round the neurotransmitter transporter. However, we did observe a correlation with fluctuations in the number of particles in a given volume, see supplementary figures S5 and S6. These changes in fluctuations were particularly strong for double bond particles, we anticipate that this effect could be related to local compressibility and heat capacity changes within the membrane.

Discussion

CG simulations have been previously used to study individual membrane proteins embedded in various lipid bilayers. These studies aimed to examine either distinct lipid propensities for the interface [48–52], or mismatches in thickness or curvature [51], particularly in the context of protein-protein interactions [54, 55, 84, 85]. They also reproduce features corresponding to the dynamical lipid annulus [86]. Here, we proposed a more systematic study of these features using an extended subset of membrane proteins in a unique environment. Also, we confronted CG simulations with the elastic model, and the dynamic annulus, the two main theoretical frameworks used to describe the relationship between membranes and their embedded proteins. Our results are both in agreement with previous simulation studies and reproduce features coming from each of the two frameworks. However, beyond this we show that the lipids close to a membrane protein are perturbed in multiple different manners, in a protein dependent manner. In agreement with the literature and the elastic vision, we observe changes in membrane thickness and curvature that relax on lengths scales of a few nanometers [42, 87]. However, this relaxation not only depends on the mismatch but also on the details of the behavior of individual lipids in the vicinity of membrane protein, giving rise to a large variety of relaxation scheme and perturbations. Unexpectedly in polar averages (see methods) other perturbations are also visible that do not correspond to these previously described effects. In particular, deviations in the relaxation of curvature and thickness near to the protein surface figure 3 can be observed and, more unexpectedly, a large perturbation and often complex relaxation over very long distances of the position of the

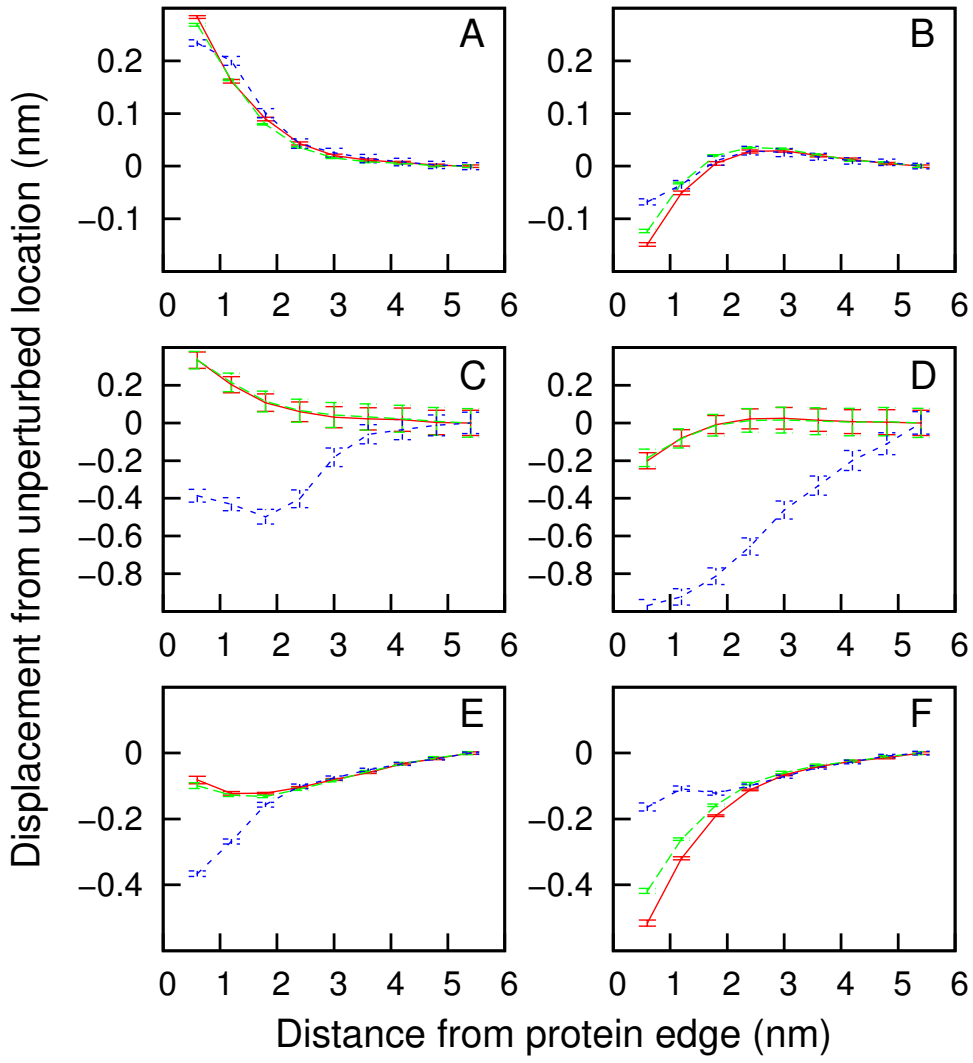

Figure 4: Profiles showing changes in the depths of different groups in the membrane as a function of the distance from the protein. Profiles are shown for the inner (A,C,E) and outer (B,D,F) leaflets of the membrane. Profiles for three different proteins are illustrated: the glycerol facilitator GlpF (PDB ID: 1FX8), panels A and B; the neurotransmitter transporter (PDB ID: 2A65), panels C and D; and lactose permease (PDB ID: 1PV6), panels E and F. Three different chemical groups are shown: the oleyl double bond (blue lines); the head group (red lines), and the glycerol (green lines).

double bond in the membrane figure4. These observations suggest that, even in a centro-symmetric field like vision of the membrane, protein-lipid interactions are much more extended, and diverse, than simply modifications in the membrane curvature and hydrophobic thickness.

In agreement with the molecular vision of protein lipid interactions we observe preferential lipid sites, figure 1, on the protein surface, and selection of lipids with certain head-groups, figure2, corresponding to bound and annular lipids. Unexpectedly we observe several other modifications in lipid structure around proteins that appear not to have been previously reported, notably multiple solvation shells figure2 and fluctuations in the position and density of the double bond in unsaturated lipid chains, figure 4 and supplementary figures S5 and S6. These unexpected novel perturbations of lipid structure and organization around the proteins we have studied also extend for long distances from the protein surface.

The perturbation observed in the position of double bond particles, which correlates with the fluctuations in the number of these particles, is particularly striking. The observation that the similar perturbation can be made for other particles, supplementary figure S5, suggests that the perturbation to the membrane properties is extensive. The fact that we can observe changes in the amplitude of fluctuations suggest that this effect may at a thermodynamic level be linked to such parameters as local compressibility ,and possibly heat capacity. However, elucidation of the molecular origins of this perturbation, both at the protein surface, and through the lipid molecular configurations, requires further work.

Furthermore, our results indicates that the molecular modifications in the solvating lipids seem to be dictated by the details of the protein surface with certain features on the surface nucleating the long range perturbations.

The composition of a biological membrane is much more complex than the membrane we have modeled. Even the relatively simple inner membrane of Gram negative bacteria contains more than two components, in particular there are about 10 mol % cardiolipins, acyl chain heterogeneity and lipid asymmetry, none of which we have considered. Most other membranes have an even more complex composition. This molecular diversity may result in more complex lipid sorting, than we have observed here. However such sorting represents an additional route to relaxing the perturbations that we have described here.

These observations have implications for the interactions between membrane proteins and their assembly. Solvent perturbation can results in attractive or repulsive forces between different solutes. To assess the importance of these forces it is necessary to evaluate the different energetic contributions. The elastic vision allows estimation of these forces using measured macroscopic parameters. While in the molecular vision estimation of forces is complex, depending as it does on thermodynamic integration or calculations of configurational entropy. Unfortunately our results would seem to indicate that while elastic forces allow an at least partial description of long range interactions they are probably less useful for estimating short range interactions.

We have previously argued that a "lipophobic" effect operating over long distances is necessary to explain the observed organization of membrane proteins [31]. Our observations here suggest that this lipophobic effect is more complex than hydrophobic and curvature mismatch and contains multiple additional aspects. These include at short distances lipid sorting and binding, and and longer distances subtle perturbations of lipid organization. In this manuscript we provide molecular view of these different types of lipid perturbation.

Acknowledgments

This work was supported by the CNRS and Aix-Marseille University and used high performance computing resources from GENCI-CINES (Grants number 2009076198, 2010076198 and 2012076198).

References

[1] M. Bogdanov, J. Xie, W. Dowhan, Lipid-protein interactions drive membrane protein topogenesis in accordance with the positive inside rule, Journal of Biological Chemistry 284 (2009) 9637–9641.

[2] M. Bogdanov, W. Dowhan, Lipid-dependent Generation of Dual Topology for a Membrane Protein., The Journal of biological chemistry 287 (2012) 37939–48.

[3] H. Vitrac, M. Bogdanov, W. Dowhan, In vitro reconstitution of lipid-dependent dual topology and postassembly topological switching of a membrane protein., Proceedings of the National Academy of Sciences of the United States of America 110 (2013) 9338–43.

[4] M. Bogdanov, W. Dowhan, H. Vitrac, Lipids and topological rules governing membrane protein assembly, Biochimica et Biophysica Acta - Molecular Cell Research 1843 (2014) 1475–1488.

[5] M. Bogdanov, P. Heacock, Z. Guan, W. Dowhan, Plasticity of lipid-protein interactions in the function and topogenesis of the membrane protein lactose permease from Escherichia coli., Proceedings of the National Academy of Sciences of the United States of America 107 (2010) 15057–62.

[6] A. Sumino, T. Dewa, T. Noji, Y. Nakano, N. Watanabe, R. Hildner, N. Bösch, J. Köhler, M. Nango, Influence of phospholipid composition on self-assembly and energy-transfer efficiency in networks of light-harvesting 2 complexes., The journal of physical chemistry. B 117 (2013) 10395–404.

[7] D. Milovanovic, A. Honigmann, S. Koike, F. Göttfert, G. Pähler, M. Junius, S. Müllar, U. Diederichsen, A. Janshoff, H. Grubmüller, H. J. Risselada, C. Eggeling, S. W. Hell, G. van den Bogaart, R. Jahn, Hydrophobic mismatch sorts SNARE proteins into distinct membrane domains, Nature Communications 6 (2015) 5984.

[8] K. Charalambous, D. Miller, P. Curnow, P. J. Booth, Lipid bilayer composition influences small multidrug transporters., BMC biochemistry 9 (2008) 31.

[9] D. N. Amin, G. L. Hazelbauer, Influence of membrane lipid composition on a transmembrane bacterial chemoreceptor., The Journal of biological chemistry 287 (2012) 41697–705.

[10] A. C. Y. Foo, B. G. R. Harvey, J. J. Metz, N. K. Goto, Influence of hydrophobic mismatch on the catalytic activity of E scherichia coli GlpG rhomboid protease, Protein Science 24 (2015) 464–473.

[11] W. Helfrich, Elastic properties of lipid bilayers: theory and possible experiments., Zeitschrift fur Naturforschung. Teil C: Biochemie, Biophysik, Biologie, Virologie 28 (1973) 693–703.
[12] O. G. Mouritsen, M. Bloom, Mattress model of lipid-protein interactions in membranes., Biophysical journal 46 (1984) 141–53.
[13] D. R. Fattal, A. Ben-shaul, A Molecular Model for Lipid-Protein Interaction in Membranes : the Role of Hydrophobic Mismatch 65 (1993).
[14] E. Sparr, W. L. Ash, P. V. Nazarov, D. T. S. Rijkers, M. A. Hemminga, D. P. Tieleman, J. A. Killian, Self-association of transmembrane alpha-helices in model membranes: importance of helix orientation and role of hydrophobic mismatch., The Journal of biological chemistry 280 (2005) 39324–31.
[15] D. Marsh, Protein modulation of lipids, and vice-versa, in membranes, Biochimica et Biophysica Acta - Biomembranes 1778 (2008) 1545–1575.
[16] A. Holt, J. A. Killian, Orientation and dynamics of transmembrane peptides: The power of simple models, European Biophysics Journal 39 (2010) 609–621.
[17] J. N. Sturgis, C. N. Hunter, R. A. Niederman, Assembly of Intracytoplasmic membranes in Rhodobacter Sphaeroides mutants lacking light-harvesting and reaction center complexes, in: G. Drews, E. A. Dawes (Eds.), Molecular Biology of Membrane-Bound Comlexes in Phototrophic Bacteria, Plenum Press, New York, 1990, pp. 219–226.
[18] a. Ben-Shaul, N. Ben-Tal, B. Honig, Statistical thermodynamic analysis of peptide and protein insertion into lipid membranes., Biophysical journal 71 (1996) 130–137.
[19] J. N. Sturgis, B. Robert, The role of chromophore coupling in tuning the spectral properties of peripheral light-harvesting protein of purple bacteria, Photosynthesis Research 50 (1996) 5–10.
[20] L. a. Bagatolli, O. G. Mouritsen, Is the fluid mosaic (and the accompanying raft hypothesis) a suitable model to describe fundamental features of biological membranes? What may be missing?, Frontiers in plant science 4 (2013) 457.
[21] A. Tonnesen, S. M. Christensen, V. Tkach, D. Stamou, Geometrical membrane curvature as an allosteric regulator of membrane protein structure and function, Biophysical Journal 106 (2014) 201–209.
[22] S. Arumugam, P. Bassereau, Membrane nanodomains: contribution of curvature and interaction with proteins and cytoskeleton., Essays in biochemistry 57 (2015) 109–19.
[23] L. Adamian, H. Naveed, J. Liang, Lipid - binding surfaces of membrane proteins: Evidence from evolutionary and structural analysis., Biochimica et biophysica acta 1808 (2010) 1092–1102.
[24] A. Laganowsky, E. Reading, T. M. Allison, M. B. Ulmschneider, M. T. Degiacomi, A. J. Baldwin, C. V. Robinson, Membrane proteins bind lipids selectively to modulate their structure and function., Nature 510 (2014) 172–5.
[25] P. L. Yeagle, Non-covalent binding of membrane lipids to membrane proteins, Biochimica et Biophysica Acta - Biomembranes 1838 (2014) 1548–1559.
[26] A. G. Lee, How lipids and proteins interact in a membrane: a molecular approach., Molecular bioSystems 1 (2005) 203–212.
[27] A. G. Lee, Lipid-protein interactions., Biochemical Society transactions 39 (2011) 761–6.
[28] S. Eggensperger, O. Fisette, D. Parcej, L. V. Schäfer, R. Tampé, An Annular Lipid Belt Is Essential for Allosteric Coupling and Viral Inhibition of the Antigen Translocation Complex TAP (Transporter Associated with Antigen Processing)., The Journal of biological chemistry 289 (2014) 33098–108.
[29] Y. Yano, K. Kondo, R. Kitani, A. Yamamoto, K. Matsuzaki, Cholesterol-Induced Lipophobic Interaction between Transmembrane Helices Using Ensemble and Single-Molecule Fluorescence Resonance Energy Transfer., Biochemistry 54 (2015) 1371–9.
[30] R. E. Jacobs, S. H. White, Lipid bilayer perturbations induced by simple hydrophobic peptides., Biochemistry 26 (1987) 6127–6134.
[31] J.-P. Duneau, J. N. Sturgis, Lateral organization of biological membranes: role of long-range interactions., European biophysics journal : EBJ 42 (2013) 843–50.
[32] C. Aponte-Santamaría, R. Briones, A. D. Schenk, T. Walz, B. L. de Groot, Molecular driving forces defining lipid positions around aquaporin-0., Proceedings of the National Academy of Sciences of the United States of America 109 (2012).
[33] P. J. Stansfeld, E. E. Jefferys, M. S. P. Sansom, Multiscale simulations reveal conserved patterns of lipid interactions with aquaporins, Structure 21 (2013) 810–819.
[34] M. C. Pitman, A. Grossfield, F. Suits, S. E. Feller, Role of cholesterol and polyunsaturated chains in lipid-protein interactions: molecular dynamics simulation of rhodopsin in a realistic membrane environment., Journal of the American Chemical Society 127 (2005) 4576–7.
[35] A. Arkhipov, Y. Shan, R. Das, N. F. Endres, M. P. Eastwood, D. E. Wemmer, J. Kuriyan, D. E. Shaw, Architecture and membrane interactions of the EGF receptor., Cell 152 (2013) 557–69.
[36] N. F. Endres, R. Das, A. W. Smith, A. Arkhipov, E. Kovacs, Y. Huang, J. G. Pelton, Y. Shan, D. E. Shaw, D. E. Wemmer, J. T. Groves, J. Kuriyan, Conformational Coupling across the Plasma Membrane in Activation of the EGF Receptor., Cell 152 (2013) 543–56.
[37] A. Arkhipov, Y. Shan, E. T. Kim, R. O. Dror, D. E. Shaw, Her2 activation mechanism reflects evolutionary preservation of asymmetric ectodomain dimers in the human EGFR family, eLife 2013 (2013) 1–14.
[38] Y. Shan, A. Arkhipov, E. T. Kim, A. C. Pan, D. E. Shaw, Transitions to catalytically inactive conformations in EGFR kinase., Proceedings of the National Academy of Sciences of the United States of America 110 (2013) 7270–5.
[39] M. Levitt, Birth and future of multiscale modeling for macromolecular systems (nobel lecture), Angewandte Chemie - International Edition (2014) 10006–10018.
[40] A. Warshel, Multiscale Modeling of Biological Functions: From Enzymes to Molecular Machines (Nobel Lecture)., Angewandte Chemie (International ed. in English) (2014) 2–14.
[41] M. Karplus, Development of multiscale models for complex chemical systems: From H+H2 to biomolecules (nobel lecture), Angewandte Chemie - International Edition (2014) 9992–10005.
[42] M. Venturoli, B. Smit, M. M. Sperotto, Simulation studies of protein-induced bilayer deformations, and lipid-induced protein tilting, on a mesoscopic model for lipid bilayers with embedded proteins., Biophysical journal 88 (2005) 1778–98.
[43] F. J.-M. de Meyer, A. Benjamini, J. M. Rodgers, Y. Misteli, B. Smit, Molecular Simulation of the DMPC-Cholesterol Phase Diagram, The Journal of Physical Chemistry B 114 (2010) 10451–10461.
[44] C. Hong, D. P. Tieleman, Y. Wang, Microsecond molecular dynamics simulations of lipid mixing., Langmuir : the ACS journal of surfaces and colloids 30 (2014) 11993–2001.
[45] H. I. Ingólfsson, M. N. Melo, F. J. V. Eerden, C. Arnarez, C. A. López, T. A. Wassenaar, X. Periole, A. H. D. Vries, D. P. Tieleman, S. J. Marrink, Lipid Organization of the Plasma Membrane Lipid Organization of the Plasma Membrane, Journal of the American Chemical Society 136 (2014) 14554–14559.
[46] S. Kawamoto, M. L. Klein, W. Shinoda, Coarse-grained molecular dynamics study of membrane fusion: Curvature effects on free energy barriers along the stalk mechanism, The Journal of Chemical Physics 143 (2015) 243112.
[47] S. Sharma, B. N. Kim, P. J. Stansfeld, M. S. P. Sansom, M. Lindau, A coarse grained model for a lipid membrane with physiological composition and leaflet asymmetry, PLoS ONE 10 (2015) 1–21.
[48] G. van den Bogaart, K. Meyenberg, H. J. Risselada, H. Amin, K. I. Willig, B. E. Hubrich, M. Dier, S. W. Hell, H. Grubmüller, U. Diederichsen, R. Jahn, Membrane protein sequestering by ionic proteinlipid interactions, Nature 479 (2011) 552–555.
[49] C. Arnarez, S. J. Marrink, X. Periole, Identification of cardiolipin binding sites on cytochrome c oxidase at the entrance of proton channels., Scientific reports 3 (2013) 1263.

[50] C. Arnarez, J.-P. Mazat, J. Elezgaray, S.-J. Marrink, X. Periole, Evidence for cardiolipin binding sites on the membrane-exposed surface of the cytochrome bc1., Journal of the American Chemical Society 135 (2013) 3112–20.

[51] D. L. Parton, A. Tek, M. Baaden, M. S. P. Sansom, Formation of Raft-Like Assemblies within Clusters of Influenza Hemagglutinin Observed by MD Simulations, PLoS Computational Biology 9 (2013).

[52] L. Janosi, Z. Li, J. F. Hancock, A. a. Gorfe, Organization, dynamics, and segregation of Ras nanoclusters in membrane domains., Proceedings of the National Academy of Sciences of the United States of America 109 (2012) 8097–102.

[53] F. J.-M. de Meyer, M. Venturoli, B. Smit, Molecular simulations of lipid-mediated protein-protein interactions., Biophysical journal 95 (2008) 1851–65.

[54] U. Schmidt, G. Guigas, M. Weiss, Cluster formation of transmembrane proteins due to hydrophobic mismatching., Physical review letters 101 (2008) 128104.

[55] L. V. Schafer, D. H. de Jong, A. Holt, a. J. Rzepiela, a. H. de Vries, B. Poolman, J. a. Killian, S. J. Marrink, Lipid packing drives the segregation of transmembrane helices into disordered lipid domains in model membranes, Proceedings of the National Academy of Sciences (2011).

[56] I. Casuso, P. Sens, F. Rico, S. Scheuring, Experimental evidence for membrane-mediated protein-protein interaction., Biophysical journal 99 (2010) L47–9.

[57] S. Scheuring, J. N. Sturgis, Chromatic adaptation of photosynthetic membranes., Science (New York, N.Y.) 309 (2005) 484–7.

[58] E. Frotscher, B. Danielczak, C. Vargas, A. Meister, G. Durand, S. Keller, A Fluorinated Detergent for Membrane-Protein Applications, Angewandte Chemie International Edition (2015) n/a–n/a.

[59] Kauzmann W., Some factors in the interpretation of protein denaturation., volume 14 of *Advances in Protein Chemistry*, Elsevier, 1959.

[60] J. Arce, J. N. Sturgis, J.-P. Duneau, Dissecting membrane protein architecture: An annotation of structural complexity., Biopolymers 91 (2009) 815–29.

[61] K. Murzyn, T. Róg, M. Pasenkiewicz-Gierula, Phosphatidylethanolamine-phosphatidylglycerol bilayer as a model of the inner bacterial membrane., Biophysical journal 88 (2005) 1091–103.

[62] W. Zhao, T. Rog, A. A. Gurtovenko, I. Vattulainen, M. Karttunen, T. Róg, A. A. Gurtovenko, I. Vattulainen, M. Karttunen, Role of phosphatidylglycerols in the stability of bacterial membranes, Biochimie 90 (2008) 930–938.

[63] L. Monticelli, S. K. Kandasamy, X. Periole, R. G. Larson, D. P. Tieleman, S.-J. Marrink, The MARTINI Coarse-Grained Force Field: Extension to Proteins, Journal of Chemical Theory and Computation 4 (2008) 819–834.

[64] D. Van Der Spoel, E. Lindahl, B. Hess, G. Groenhof, A. E. Mark, H. J. C. Berendsen, GROMACS: fast, flexible, and free., Journal of computational chemistry 26 (2005) 1701–18.

[65] M. G. Wolf, M. Hoefling, C. Aponte-Santamaría, H. Grubmüller, G. Groenhof, g_membed: Efficient insertion of a membrane protein into an equilibrated lipid bilayer with minimal perturbation., Journal of computational chemistry 31 (2010) 2169–74.

[66] X. Periole, M. Cavalli, S.-J. Marrink, M. A. Ceruso, Combining an Elastic Network With a Coarse-Grained Molecular Force Field: Structure, Dynamics, and Intermolecular Recognition, Journal of Chemical Theory and Computation 5 (2009) 2531–2543.

[67] H. J. C. Berendsen, J. P. M. Postma, W. F. van Gunsteren, a. DiNola, J. R. Haak, Molecular dynamics with coupling to an external bath, The Journal of Chemical Physics 81 (1984) 3684–3690.

[68] W. Humphrey, VMD: Visual molecular dynamics, Journal of Molecular Graphics 14 (1996) 33–38.

[69] R. Dutzler, E. B. Campbell, R. MacKinnon, Gating the selectivity filter in ClC chloride channels., Science (New York, N.Y.) 300 (2003) 108–112.

[70] J. K. Lee, D. Kozono, J. Remis, Y. Kitagawa, P. Agre, R. M. Stroud, Structural basis for conductance by the archaeal aquaporin AqpM at 1.68 A., Proceedings of the National Academy of Sciences of the United States of America 102 (2005) 18932–18937.

[71] C. Hunte, E. Screpanti, M. Venturi, A. Rimon, E. Padan, H. Michel, Structure of a Na+/H+ antiporter and insights into mechanism of action and regulation by pH., Nature 435 (2005) 1197–1202.

[72] D. Fu, a. Libson, L. J. Miercke, C. Weitzman, P. Nollert, J. Krucinski, R. M. Stroud, Structure of a glycerol-conducting channel and the basis for its selectivity., Science (New York, N.Y.) 290 (2000) 481–486.

[73] S. Törnroth-Horsefield, Y. Wang, K. Hedfalk, U. Johanson, M. Karlsson, E. Tajkhorshid, R. Neutze, P. Kjellbom, Structural mechanism of plant aquaporin gating., Nature 439 (2006) 688–694.

[74] J. Abramson, I. Smirnova, V. Kasho, G. Verner, H. R. Kaback, S. Iwata, Structure and mechanism of the lactose permease of Escherichia coli., Science (New York, N.Y.) 301 (2003) 610–615.

[75] Y. Huang, M. J. Lemieux, J. Song, M. Auer, D.-N. Wang, Structure and mechanism of the glycerol-3-phosphate transporter from Escherichia coli., Science (New York, N.Y.) 301 (2003) 616–620.

[76] K. P. Locher, A. T. Lee, D. C. Rees, The E. coli BtuCD structure: a framework for ABC transporter architecture and mechanism., Science (New York, N.Y.) 296 (2002) 1091–1098.

[77] E. Pebay-Peyroula, C. Dahout-Gonzalez, R. Kahn, V. Trézéguet, G. J.-M. Lauquin, G. Brandolin, Structure of mitochondrial ADP/ATP carrier in complex with carboxyatractyloside., Nature 426 (2003) 39–44.

[78] Y. Zhou, R. MacKinnon, The occupancy of ions in the K+ selectivity filter: Charge balance and coupling of ion binding to a protein conformational change underlie high conduction rates, Journal of Molecular Biology 333 (2003) 965–975.

[79] A. Yamashita, S. K. Singh, T. Kawate, Y. Jin, E. Gouaux, Crystal structure of a bacterial homologue of Na+/Cl–dependent neurotransmitter transporters., Nature 437 (2005) 215–223.

[80] G. E. Tusnády, Z. Dosztányi, I. Simon, Transmembrane proteins in the Protein Data Bank: identification and classification., Bioinformatics (Oxford, England) 20 (2004) 2964–72.

[81] D. Kozma, I. Simon, G. E. Tusnady, PDBTM: Protein Data Bank of transmembrane proteins after 8 years, Nucleic Acids Research 41 (2013) D524–D529.

[82] C. Aponte-Santamaría, R. Briones, A. D. Schenk, T. Walz, B. L. de Groot, Molecular driving forces defining lipid positions around aquaporin-0., Proceedings of the National Academy of Sciences of the United States of America 109 (2012) 9887–92.

[83] M. A. Lomize, I. D. Pogozheva, H. Joo, H. I. Mosberg, A. L. Lomize, OPM database and PPM web server: Resources for positioning of proteins in membranes, Nucleic Acids Research 40 (2012) 370–376.

[84] X. Periole, T. Huber, S.-J. Marrink, T. P. Sakmar, G protein-coupled receptors self-assemble in dynamics simulations of model bilayers., Journal of the American Chemical Society 129 (2007) 10126–32.

[85] F. de Meyer, B. Smit, Comment on "Cluster formation of transmembrane proteins due to hydrophobic mismatching"., Physical review letters 102 (2009) 219801; author reply 219802.

[86] P. S. Niemelä, M. S. Miettinen, L. Monticelli, H. Hammaren, P. Bjelkmar, T. Murtola, E. Lindahl, I. Vattulainen, Membrane proteins diffuse as dynamic complexes with lipids, Journal of the American Chemical Society 132 (2010) 7574–7575.

[87] S. Mondal, H. Weinstein, G. Khelashvili, 9.12 Interactions of the Cell Membrane with Integral Proteins, in: Comprehensive Biophysics, volume 9, Elsevier, 2012, pp. 229–242.

Supplementary data

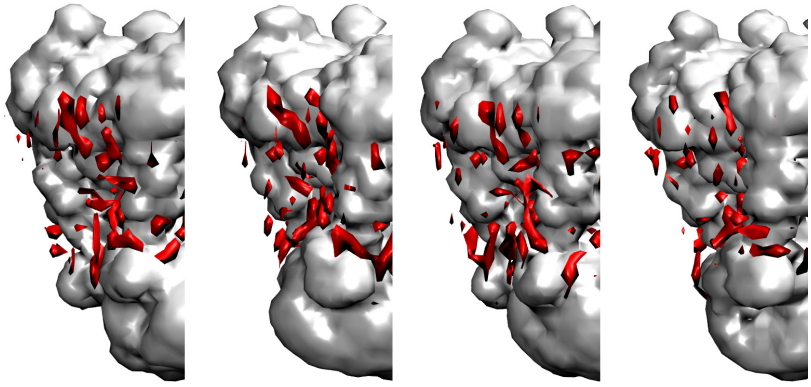

Figure S1: Lipids on the surface of the Potassium channel KcsA. Lipid locations on the surface of the protein for the four monomers in the KcsA tetramer, showing the convergence of density and its dependence on the details of the protein topography. As in figure 1 particle densities were averaged from 2500 frames sampled from the 10 μs of simulation. The red surfaces show zones of density greater than 1.36 times the average lipid particle density in the membrane.

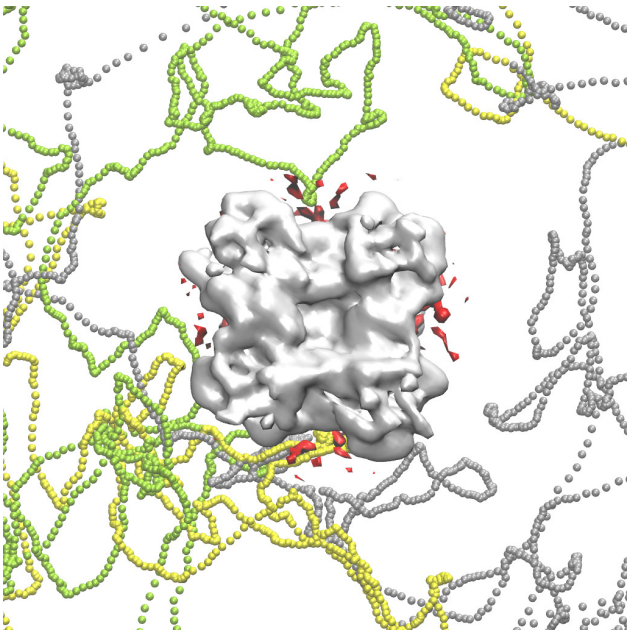

Figure S2: Trajectories of three selected lipids that bind on the surface of the Potassium channel KcsA (viewed from the extracellular side), at the site illustrated in figure 1, sampled in every 4 ns. The green trace corresponds to a single lipid that visited the site on 3 of the 4 monomers. The surface density patches are the same as in figure 1 and supplementary figure S1.

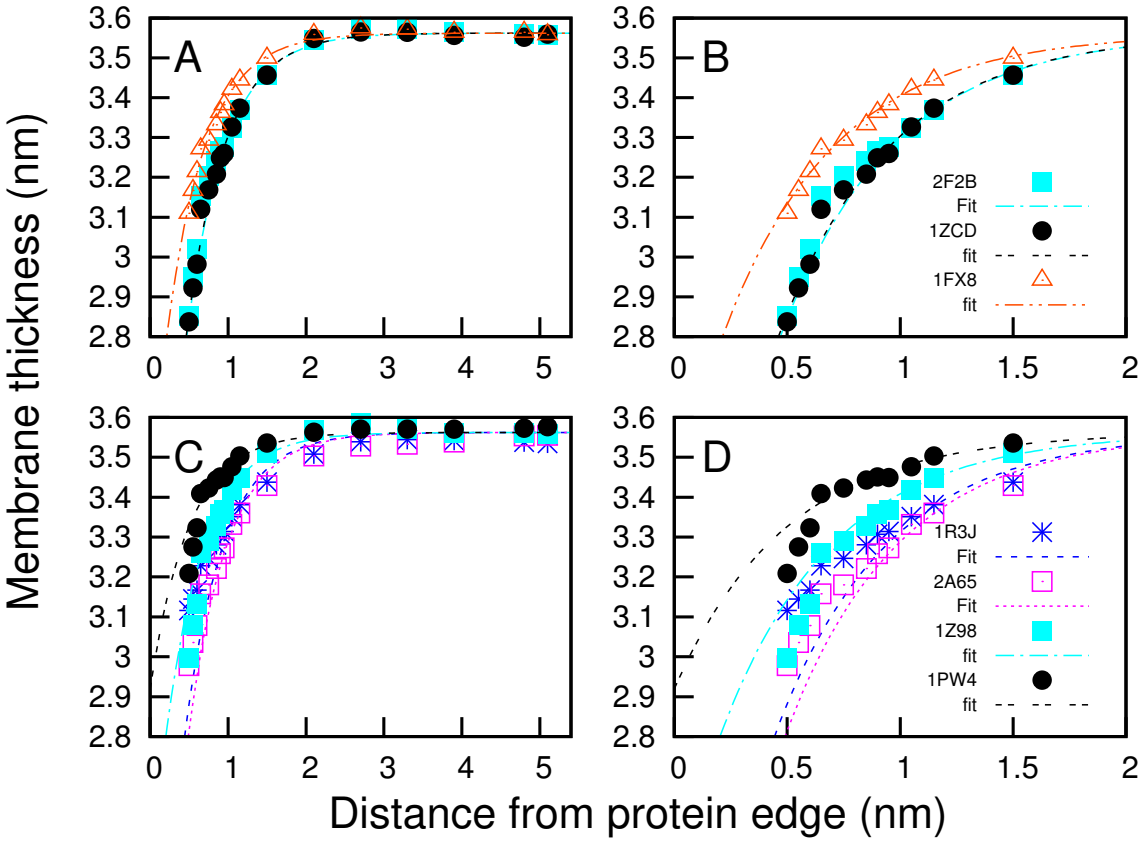

Figure S3: Relaxation of membrane thickness as distance from the protein surface increases. Membrane thickness, was calculated as the distance between the glycerol moieties of the phospholipids and is show as a function of the distance from the protein surface for the protein. The lines show exponential fits to the data, with the parameters shown in table 2. The left panels show data going out to long distances while right panels concentrate on the distortions close to the protein. Panels A and B correspond to 3 proteins that can be well fitted from long distance to the first shell of lipids using a simple elastic model of membrane thickness: aquaporin M 2F2B turquoise, the sodium proton antiporter 1ZCD, black; the glycerol facilitator GlpF 1FX8 red. Panels C and D correspond to 4 other proteins for which thickness relaxation at the protein boundary can not be extrapolated from long range relaxation: the Glycerol 3 phosphate transporter 1PW4, black; the spinach aquaporin SoPIP2 1Z98, turquoise; 2A65, red; the potassium transporter KcsA 1R3J, blue.

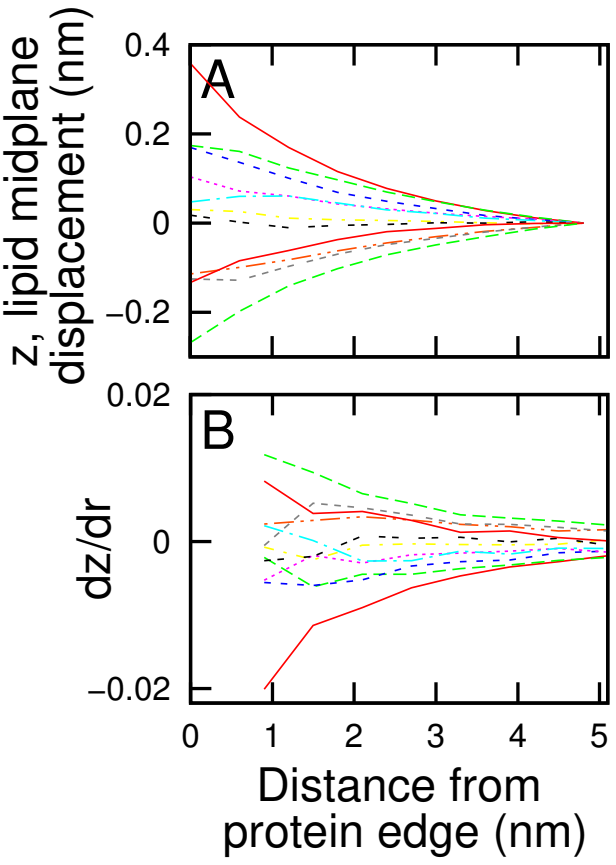

Figure S4: Membrane curvature. Displacement of the membrane mid-plane (panel A) was calculated assuming a centro-symmetric model as a function of distance from the protein center, and the derivative of this with distance (panel B). From upper to lower curve (left edge of panel A), the 1A proteins pdb codes are: 1R3J, 1L7V, 2F2B, 2A65, 1FX8, 1Z98, 1ZCD, 1OKC, 1PW4, 1OTS and 1PV6.

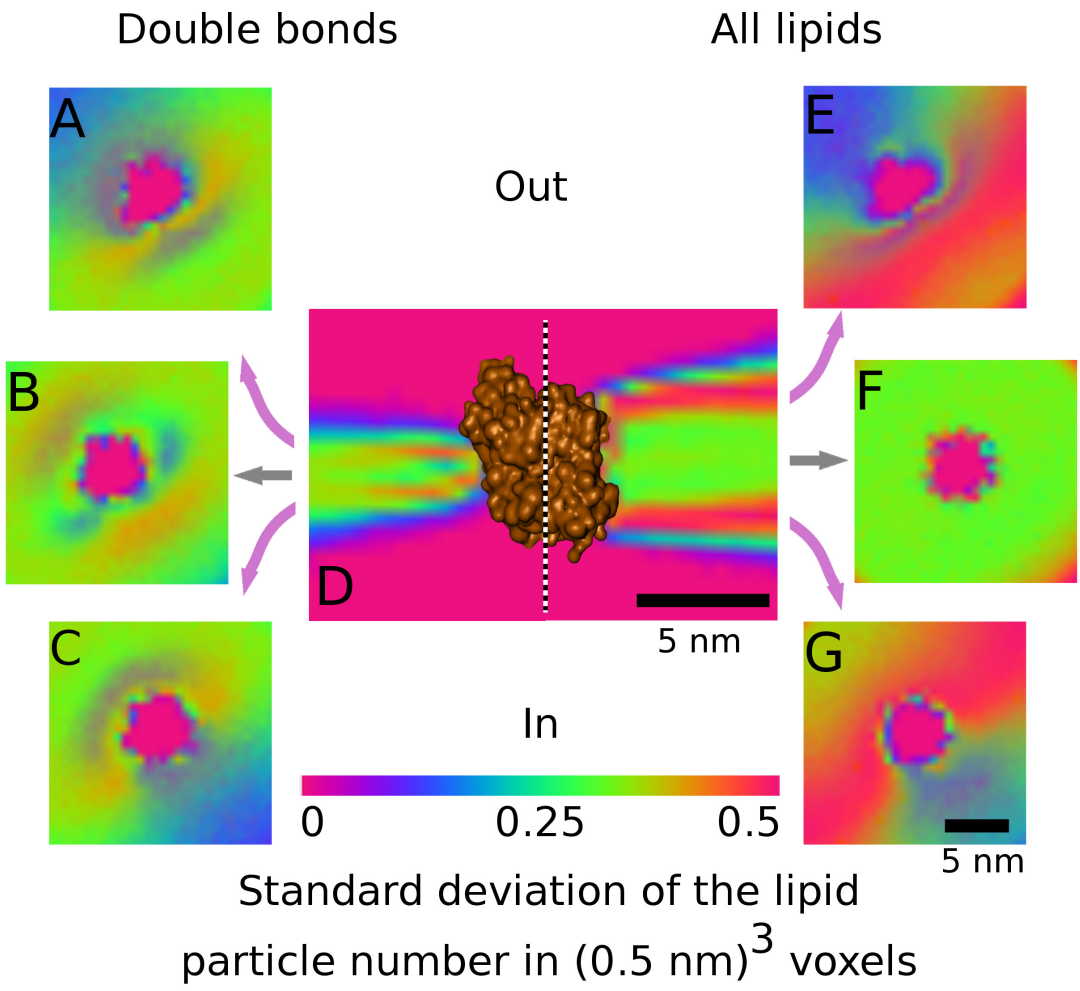

Figure S5: Fluctuation of particle number in voxels around the neurotransmitter transporter system (PDB ID: 2A65). Fluctuations were computed using 0.125 nm3 boxes and either considering double bond beads (left) or to all lipid beads (right). The results are shown for the center plane of the membrane (panels B and F) or for planes corresponding to maximum of density for each group of particle (A, C and E, G). The position of these planes are illustrated using the longitudinal section of the system (panel D).

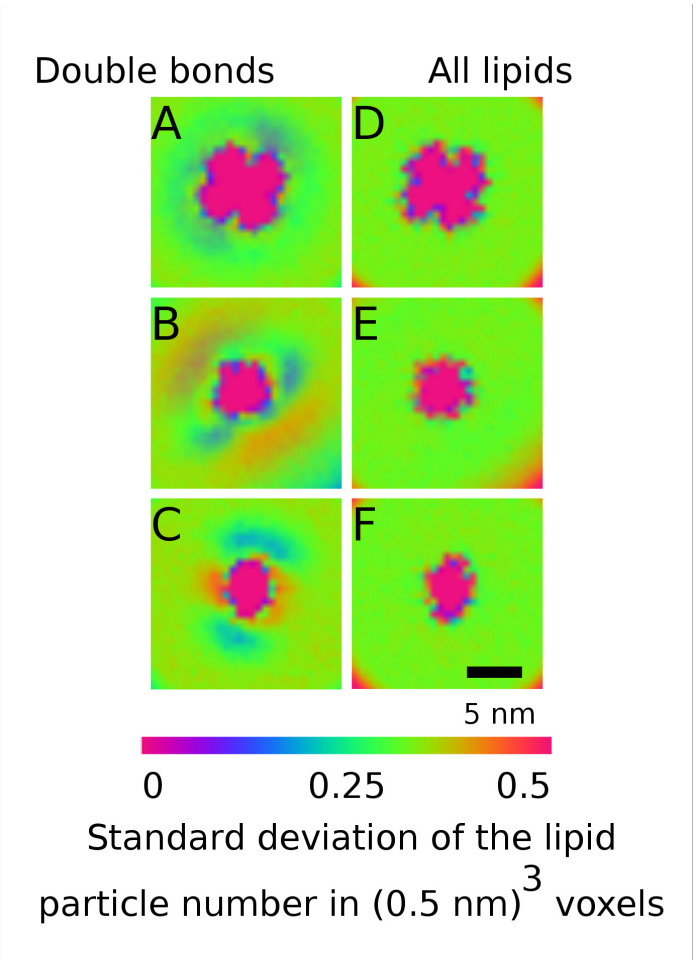

Figure S6: Fluctuation of particle number in the central plane of the different system considered in figure 4: the glycerol facilitator GlpF (PDB ID: 1FX8), panels A and B; the neurotransmitter transporter (PDB ID: 2A65), panels C and D; and the lactose permease (PDB ID: 1PV6), panels E and F. The fluctuation either corresponds to double bond beads (left; panel A, B, C) or to all lipid beads (right; panel D, E, F).